DESIGN AND CONTROL OF A SIMPLIFIED STEWART PLATFORM FOR ENDOSCOPY

Jeff M. Wendlandt S. Shankar Sastry

Intelligent Machines and Robotics Laboratory
University of California at Berkeley

ABSTRACT

This paper presents the development of a workspace controller for a newly designed platform. The platform is designed to manipulate endoscopic tools and is actuated by tendons to meet the small scale requirements in endoscopy. The tendon actuation provides challenges to the controller design since the number of degrees of freedom equals the number of tendons. In typical tendon-driven systems, the number of tendons is greater than the number of degrees of freedom. This paper presents the kinematic and dynamic analysis of the manipulator and presents a workspace controller for the tendon driven system. Simulation as well as experimental results are presented for the controlled system. The results demonstrate the effectiveness of the controller in tracking a step response and a circular trajectory at 2.0Hz and greater. The device is similar to the Stewart platform and the basic design can be used in applications where the full range of motion of the Stewart platform is not required. Applications of the device range between targeting systems, snake-like robots, and endoscopy.

1. Introduction

This paper presents the kinematics, dynamics and control of a tendon-driven manipulator originally designed for minimally invasive surgery. Simulation as well as experimental results are presented. The design shares similarities with the Stewart Platform but has three fewer degrees of freedom (DOF) and three fewer actuators. The manipulator is a wrist-like manipulator and provides the ability to point a tool at a desired location. The device is useful for applications which do not need the full motion of the Stewart platform.

The device is originally designed as a manipulator for endoscopy [7]. Endoscopy is a minimally invasive surgical procedure used to examine and operate in the gastrointestinal tract. The working prototype called the endo-platform is shown in Figure 1. It consists of two platforms separated by rigid tubes and a spring-like device attaching the tubes. The spring serves as a spherical joint which resists twisting about the axis of the tubes. Three tendons are attached to the outer plate. A tool, such as a biopsy forceps, runs through the centers of the plates. Pulling on the tendons changes the orientation of the outer plate and results in the motion of the tool. In this way, surgeons are able to control the pointing direction of the tool. The plates are designed to have the same diameter as endoscopes which are typically 10mm.

Actuation is accomplished by tendons to meet the size restrictions inherent in the application. The use of tendons adds challenges to the controller design because the tendons can exert force in only one direction. In typical tendon-driven systems, there are more actuators than degrees of freedom. In this system, there are three tendons for three degrees of freedom and this fact adds additional challenges to the controller. One DOF is for twisting about the central axis and two DOF are for pointing the tool.

Research supported in part by an NSF graduate fellowship and NIH under grant R03RR06996. wents@eecs.berkeley.edu

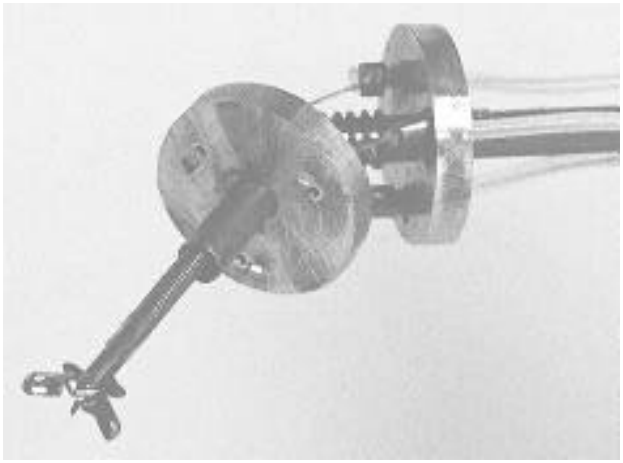

Figure 1: Endo-Platform with Forceps

Originally developed for endoscopy, this design can be used in other applications where the control of the pointing direction of a tool or instrument is desired. The elimination of the space restrictions allows more freedom in the mechanical design. For example, one can replace the spring-like device with a constant velocity joint, commonly used in front wheel drive automobiles . The constant velocity joint resists twists if the inner shaft is held fixed relative to the inner plate and allows the outer plate to orient relative to the inner plate. Linear or hydraulic actuators which produce force in both directions can replace the tendons.

The original design which led to the endo-platform design is similar to a design in [3] which attaches an elastic tube between two plates. The rigid tubes and the spring used in the endo-platform approximate a spherical joint about a fixed point. The pivot point resists side forces better than the elastic tube design. Also, pivoting at a point instead of bending the entire tube uses less space transversal to the tool axis as the tool is pointed. As in [3], the platforms can be combined to create a snake-like robot.

The first section after the introduction presents the

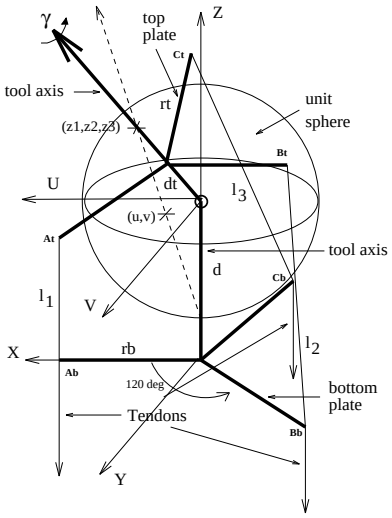

Figure 2: Kinematic Model

kinematic model along with the kinematic analysis. Special coordinates are selected which simplify the dynamic analysis presented in Section 3. Section 4 presents a control algorithm which uses the kinematic model and the dynamic model. This controller can be simplified for use with hydraulic or linear actuators since these actuators can exert force in two directions. Section 5 presents simulation and experimental results of the controlled tendon-driven system for a step response in the desired tool coordinates and for the tracking of a circular trajectory at 2.0Hz. The resulting forces in the tendons are shown as well as the trajectories in the tool coordinates.

2. Kinematic Model and Analysis

The kinematic model of the device is shown in Figure 2. In this model, the top plate and the bottom plate are connected through a spherical joint. The three lines in the top plate which radiate from a central point connect the tool axis to the points where the tendons are attached. Similarly, the bottom plate has three radial lines attaching the bottom tool axis to the locations where the tendons pass through the bottom plate. The length of the radial lines is rt for the top plate and rb for the bottom plate. The distance from the bottom plate to the pivot point is d, and the distance from the top plate to the pivot point is dt. These four parameters characterize the particular geometry of the manipulator.

The tendons are fixed to the top plate but slide through the points in the bottom plate. The tendon lengths between the top and bottom plates are l_1, l_2, and l_3. The tool axis runs through the center of both plates. The radial lines are equally spaced 120 degrees apart and lie in the plane formed by the three points where the tendons are attached. The tendons are fixed to the top plate and are strung through the bottom plate. The orientation of the top plate is controlled by pulling on the tendons. The pointing direction is controlled by controlling the orientation of the top plate since the tool points in a direction normal to the surface of the top plate.

The tool position is given by three coordinates, (u, v, γ). The three coordinates are grouped into the vector, θ. Three frames are considered for the following kinematic analysis. There are two spatial frames and one body frame attached to the top plate. The XYZ frame is attached to the bottom plate and the UVZ frame is fixed relative to the XYZ frame and is originally coincident with the body frame in the home configuration. The home configuration is when the tool is pointing along the spatial Z axis.

The first two coordinates, u and v, correspond to a modified stereographic projection and the third coordinate, γ, corresponds to twist about the tool axis. One forms the u and v coordinates by intersecting the tool axis with a unit sphere centered about the pivot point. The line from the south pole of the sphere to the intersection point intersects the UV plane. The coordinates of the point of intersection with the plane is the (u, v) coordinates. One can reach any pointing direction given by the u, v coordinates by rotating the top plate about an axis lying in the UV plane. This is called a nontwist rotation. One can then perform a rotation about the body tool axis to reach any tool frame obtained by performing an arbitrary rotation of the UVZ axis. The amount of rotation needed about the tool axis is the coordinate γ. The home configuration of the tool is given by $(u, v, \gamma) = 0$.

The rotation matrix which represents the top plate orientation with respect to the UVZ frame in terms of u, v, and γ is now described. The map from coordinates in the unit sphere to coordinates in the UV plane is

$$(u, v) = \frac{1}{1 + z_3} (z_1, z_2) . \tag{1}$$

The coordinates in the unit sphere are (z_1, z_2, z_3). This result follows easily from similar triangles. Notice that the map is not defined when $z_3 = -1$. The inverse map is given by

$$(z_1, z_2, z_3) = (ut, vt, t - 1) \tag{2}$$

where $t = \frac{2}{1+u^2+v^2}$. As stated in [2], the rotation matrix formed by rotating about an axis $\mathbf{k} = (k_x, k_y, k_z)^T$ by an angle ϕ is given by

$$Rot(\mathbf{k}, \phi) = \begin{bmatrix} k_x k_x v_\phi + c_\phi & k_y k_x v_\phi - k_z s_\phi & k_z k_x v_\phi + k_y s_\phi \\ k_x k_y v_\phi + k_z s_\phi & k_y k_y v_\phi + c_\phi & k_z k_y v_\phi - k_x s_\phi \\ k_x k_z v_\phi - k_y s_\phi & k_y k_z v_\phi + k_x s_\phi & k_z k_z v_\phi + c_\phi \end{bmatrix} \tag{3}$$

where $c_\phi = cos(\phi)$, $s_\phi = sin(\phi)$, and $v_\phi = 1 - c_\phi$. The no twist rotation which rotates the tool axis from the vertical direction corresponds to a rotation about a unit vector lying in the UV plane. This vector is the normalized vector resulting from the cross product between the vertical axis and the current body tool axis. The axis of rotation is then

$$\mathbf{k} = \frac{1}{\sqrt{z_1^2 + z_2^2}} \begin{bmatrix} -z_2 \\ z_1 \\ 0 \end{bmatrix} . \tag{4}$$

The angle of rotation is the angle the current body axis makes with the vertical axis (see Figure 3). Using the relationships,

$$\begin{aligned} c_\phi &= z_3 \\ s_\phi &= \sqrt{z_1^2 + z_2^2} \\ v_\phi &= 1 - z_3, \end{aligned} \tag{5}$$

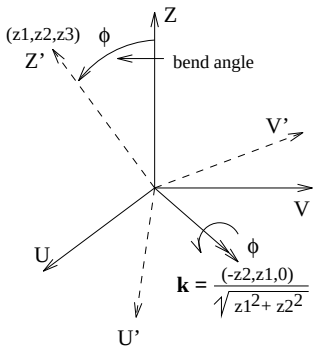

Figure 3: No Twist Rotation

and (4) and substituting into (3) yields the no-twist rotation matrix in terms of the coordinates in the sphere,

$$R_{nt}(z_1,z_2,z_3) = \begin{bmatrix} \frac{z_2^2}{1+z_3}+z_3 & \frac{-z_1z_2}{1+z_3} & z_1 \\ \frac{-z_1z_2}{1+z_3} & \frac{z_1^2}{1+z_3}+z_3 & z_2 \\ -z_1 & -z_2 & z_3 \end{bmatrix}. \quad (6)$$

Using (2) and substituting into (6) gives

$$R_{nt}(u,v) = \frac{t}{2}\begin{bmatrix} 1-u^2+v^2 & -2uv & 2u \\ -2uv & 1+u^2-v^2 & 2v \\ -2u & -2v & 1-u^2-v^2 \end{bmatrix}. \quad (7)$$

The rotation matrix which maps points in the body frame to points in the spatial UVZ frame is

$$R(u,v,\gamma) = R_{nt}(u,v)\,R_z(\gamma),$$

where

$$R_z(\gamma) = \begin{bmatrix} c_\gamma & -s_\gamma & 0 \\ s_\gamma & c_\gamma & 0 \\ 0 & 0 & 1 \end{bmatrix}. \quad (8)$$

The tendon lengths between the top and bottom plates are calculated as follows: The distance is calculated between the points A_b and A_t, B_b and B_t, and C_b and C_t defined in Figure 2. The position of the points in the top frame with respect to the UVZ frame is obtained by mapping the points through the rotation matrix. The coordinates of the points are easily determined in the XYZ spatial frame. The distances are then calculated by determining the magnitude of the vector joining the two points in the XYZ frame. This procedure defines a map from (u,v,γ) to (l_1,l_2,l_3) space. This function and its differential are contained in [7]. Assuming that $\gamma = 0$ for all time results in a jacobian which is a 3×2 matrix.

The body angular velocity is needed for the determination of the kinetic energy used in calculating the dynamic equations. The body angular velocity, ω_b, written as a skew-symmetric matrix is $\hat{\omega}_b = R^T\dot{R}$. See [5] for more details on this description of the body angular velocity. Carrying out the calculations in Mathematica [8] results in the following expression:

$$\omega_b = \begin{bmatrix} t(\dot{u}\sin(\gamma) - \dot{v}\cos(\gamma)) \\ t(\dot{u}\cos(\gamma) + \dot{v}\sin(\gamma)) \\ \dot{\gamma} + t(\dot{u}v - u\dot{v}) \end{bmatrix}. \quad (9)$$

This completes the development of the kinematics.

3. Dynamic Model

The robot dynamic equations are developed in this section. The robot dynamics are of the form

$$M(\theta)\,\ddot{\theta} + C(\dot{\theta},\theta)\dot{\theta} + N(\theta) = \tau = J^T(\theta)\,F \quad (10)$$

where $\theta = (u,v,\gamma)^T$, $M(\theta)$ is the mass matrix, $C(\dot{\theta},\theta)$ is the Coriolis matrix, and $N(\theta)$ is the vector of potential forces. The torque in the tool coordinates is denoted by τ. The vector of tendon forces is F. The jacobian of the function discussed in the kinematic section relates F to τ. Frequently, N is a function of $\dot{\theta}$ when there are dissipative and frictional forces. The model developed in this section does not include dissipative, frictional forces, nor gravitational forces.

The mass matrix is calculated from the relationship that Kinetic Energy $= \frac{1}{2}\omega_b^T\mathbb{I}\omega_b = \frac{1}{2}\dot{\theta}^T M(\theta)\,\dot{\theta}$, where $\mathbb{I}$ is the inertia matrix. The inertias are calculated along the principal axes resulting in a diagonal inertia matrix. The fact that the inertia about the U axis is equal to the inertia about the V axis simplifies the mass matrix by removing dependence of the mass matrix on γ. The moment of inertia about the U axis and the V axis is j_1 and the moment of inertia about the Z axis is j_3. Performing this calculation reveals that

$$M(\theta) = \begin{bmatrix} \frac{4(j_1+j_3v^2)}{(1+u^2+v^2)^2} & \frac{-4j_3uv}{(1+u^2+v^2)^2} & \frac{2j_3v}{1+u^2+v^2} \\ \frac{-4j_3uv}{(1+u^2+v^2)^2} & \frac{4(j_1+j_3u^2)}{(1+u^2+v^2)^2} & \frac{-2j_3u}{1+u^2+v^2} \\ \frac{2j_3v}{1+u^2+v^2} & \frac{-2j_3u}{1+u^2+v^2} & j_3 \end{bmatrix}. \quad (11)$$

The symbolic inverse of the mass matrix is then

$$M^{-1}(\theta) = \begin{bmatrix} \frac{(1+u^2+v^2)^2}{4j_1} & 0 & \frac{-v(1+u^2+v^2)}{2j_1} \\ 0 & \frac{(1+u^2+v^2)^2}{4j_1} & \frac{u(1+u^2+v^2)}{2j_1} \\ \frac{-v(1+u^2+v^2)}{2j_1} & \frac{u(1+u^2+v^2)}{2j_1} & \frac{1}{j_3}+\frac{u^2+v^2}{j_1} \end{bmatrix}. \quad (12)$$

The Coriolis matrix is derived from the mass matrix by the following formula for the ijth element. See [5] for a derivation.

$$C_{ij}(\dot{\theta},\theta) = \frac{1}{2}\sum_{k=1}^{n}\left(\frac{\partial M_{ij}}{\partial\theta_k} + \frac{\partial M_{ik}}{\partial\theta_j} - \frac{\partial M_{jk}}{\partial\theta_i}\right)\dot{\theta_k}. \quad (13)$$

Performing these calculations and multiplying on the right by the vector $\dot{\theta}$ produces the Coriolis vector.

The vector of potential forces is the force from the spring at the spherical joint. The spring resists torsional motion as well as bending motion. The spring model in this analysis assumes that the spring torsional torque is proportional to the angle of the twist, γ. The model also assumes that the torque about the pure bending axis, the axis lying in the UV plane, is proportional to the angle the tool makes with the vertical axis. See Figure 3 for a description of the pure bending axis. This relationship must be transformed into a force in the (u,v) coordinates. Using the equations in (1) and (5), one can show that

$$r := \sqrt{u^2+v^2} = \frac{\sin(\phi)}{1+\cos(\phi)}. \quad (14)$$

The spring model assumes that a torque about the pivot axis is proportional to the angle from the vertical axis. In other words,

$$\tau_\phi = K_\phi\phi. \quad (15)$$

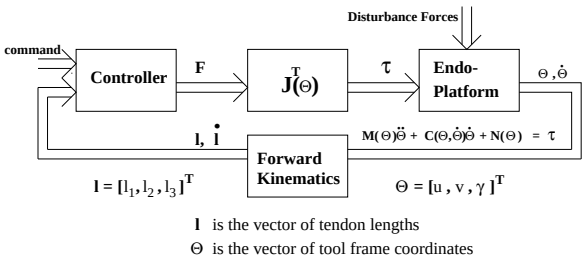

Figure 4: System Block Diagram

The inverse of (14) is

$$\phi = \cos^{-1}\left(\frac{1-r^2}{1+r^2}\right). \tag{16}$$

The inverse is obtained by substituting (5) into $\sin(\phi)$ in (14) and then using (2) in the result. The resulting expression is then solved for ϕ. The work done in either system is the same in both coordinate systems. Therefore,

$$K_\phi\ \phi\, \mathrm{d}\phi = F_r\ \mathrm{d}r.$$

This implies that

$$K_\phi\ \phi\ \frac{\mathrm{d}\phi}{\mathrm{d}r} = F_r. \tag{17}$$

Using (17) and (16) results in the following expression for the radial force

$$F_r = K_\phi\ \cos^{-1}\left(\frac{1-r^2}{1+r^2}\right)\ \frac{2}{1+r^2}. \tag{18}$$

The potential force term in the u and v directions is the radial force projected into these two directions. The complete term is then

$$N(\theta) = \begin{bmatrix} F_r(r)\ u/r \\ F_r(r)\ v/r \\ K_\gamma\ \gamma \end{bmatrix}, \tag{19}$$

where r is given in (14).

4. Control Algorithm

The control algorithm is presented in this section. The relationship between the controller, the platform, and the disturbances is shown in Figure 4. The fact that the system is driven through tendons provides a challenge to design an effective controller. Typically in tendon-driven systems, there are more actuators than degrees of freedom. In the endo-platform, there are the same number of degrees of freedom as the number of tendons.

In the home configuration, the tendons cannot exert a torque about the twist axis since the bottom row of the jacobian transpose is zero. This leads one to ignore this degree of freedom and control the two coordinates involved in the bending, (u, v). We are then interested in two degrees of freedom and have three actuators that can exert force in only one direction. The control algorithm controls in the workspace coordinates, (u, v), and computes a desired force in these coordinates. The workspace force is then mapped into tendon forces. Forces which lie in the null space of the jacobian transpose are added to

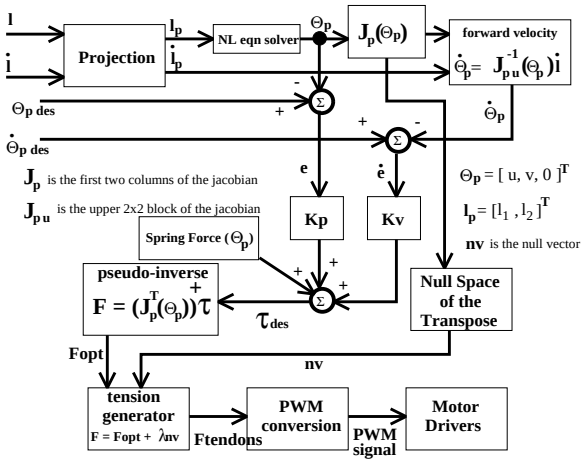

Figure 5: Control Algorithm Diagram

provide tension in the three tendons. The forces may affect the torque about the twist axis but the spring in the spherical joint is designed to resist twist.

The control algorithm is shown in Figure 5. Since we are ignoring the twist angle in the controller and assume that it is zero for the calculations, the three tendon lengths are dependent. The available information is the length of the tendons and their velocities. This is provided by optical encoders that are attached to the motors which drive the tendons. This information is used to calculate the tool coordinates as well as the velocity of the tool in these coordinates.

The inverse kinematics of the platform are solved easily while the forward kinematics are difficult to solve. This also occurs in the Stewart platform. See [6] for more details on the Stewart platform. The equations relating the tool coordinates are nonlinear and difficult to invert. The equations are in the appendix of [7]. The controller numerically solves for the roots of polynomials and produces a vector, $\theta_p := (u, v, 0)^T$. The first two columns of the jacobian are calculated with θ_p. The third column is ignored since we assume that $\gamma = 0$. The new 3×2 jacobian is defined to be $J_p(\theta_p)$. The velocity of the length of the tendons and ${J_p}^{-1}(\theta_p)$ are used to calculate the velocity in the tool coordinates assuming no twist. This velocity is $\dot{\theta_p}$. This is similar to the method of calculating the velocity in [6].

The velocity and the position information are subtracted from the desired trajectory and an error, $\mathbf{e} = \theta_{pdes} - \theta_p$, and error velocity, $\dot{\mathbf{e}}$, are formed. The error and error velocity pass through gain matrices to produce a desired torque in the tool coordinates. The spring force in the current configuration is computed and is added to the desired torque from the PD controller. This is a modified PD controller described in [5] however the inertial and Coriolis forces are ignored in this particular controller.

The equation for the torque in tool coordinates is

$$\tau = K_p e + K_v \dot{e} + N(\theta_p). \tag{20}$$

The pseudo inverse of ${J_p}^T(\theta_p)$ is used to calculate the optimal force, a force with no component in the null space of ${J_p}^T(\theta_p)$ which maps to τ. The pseudo inverse is denoted $\left({J_p}^T(\theta_p)\right)^+$. The null space of ${J_p}^T(\theta_p)$ is calculated. The null space is one dimensional, and the null vector is de-

noted nv. The coefficient, λ, is calculated so that the sum in (21) produces tension forces in the three tendons above a tension offset.

$$F_{\text{tendons}} = \left(J_p{}^T(\theta_p)\right)^+ \tau + \lambda\, nv \tag{21}$$

This is the same method described in [1] for producing tendon forces in tension. Tension is a negative force since it decreases the length of the tendon. The desired tendon force is then converted to a pulse width modulated signal to produce a torque in the motors.

This controller subtracts force in the tendons without changing the torque in the tool coordinates. This can always be accomplished if the null space is spanned by a vector with entries with the same sign. Depending on the geometry, this will not occur for certain configurations of the tool. See [7] for more details.

5. Simulation and Experimental Results

The system was simulated in Mathematica [8] with parameters measured from the prototype shown in Figure 1. The spring model in (19) was used in the controller and in the dynamic model. The current parameters are $d = 0.8$cm, $dt = 0.5$cm, $rt = 0.6$cm, and $rb = 0.6$cm. The gain matrices are diagonal and have the same coefficient along the diagonal. The kp gain is 26,356g cm/(cm s^2) and kv is 663g cm s/(cm s^2). The inertia's were calculated to be $j_1 = j_2 = 2.08$g cm^2 and $j_3 = 1.78$g cm^2. The spring constants were experimentally determined and are $k_\phi = 100,000$g cm^2/(s^2 cm) and $k_\gamma = 112,000$g cm/(s^2 rad). With an endoscopic biopsy forcep inserted into the tool channel, k_ϕ is measured to be $286,000$g cm^2/(s^2 cm) in the $+u$ direction and $517,000$g cm^2/(s^2 cm) in the $-u$ direction. In the simulation and in the experiment, k_ϕ is taken to be $400,000$g cm^2/(s^2 cm), the rounded average. Lynx, a real-time unix operating system donated from Lynx Real-Time Systems, Inc., runs the control loop at 500Hz on a 486DX-33MHz IBM clone.

The PD gains were designed in Matlab [4] using the linear quadratic regulator based on the linear error dynamics at the origin. The controller used in the experiment and in the simulation differ in that the feedforward term in the simulation is a function of the current configuration and is a function of the desired position in the experimental controller. This resulted in quicker responses. Also, the current configuration feedforward controller often could not overcome the stiction forces at the origin. The simulated response and the experimental response in position is shown in Figure 6 when the tool is commanded to step to $u = 0.3$cm and $v = 0.2$cm. The upper graphs are the u coordinate and the lower graphs are the v coordinate. The lowest graph is the twist angle as predicted by the simulation. Notice that the twist angle is nonzero and is approximately 0.01rad.

The response in the UV plane parameterized by time is shown in Figure 7. The curl in the simulation and in the experiment may be due to the nonzero twist angle which modifies how the tendon forces effect the outer plate of the endo-platform. The experimental controller with the modified feedforward term has a quicker response and settles faster than the simulation at the expense of greater tendon forces shown in Figure 8.

The experimental system is forced to track a circle of radius 0.3cm in the UV plane at a frequency of 2.0Hz.

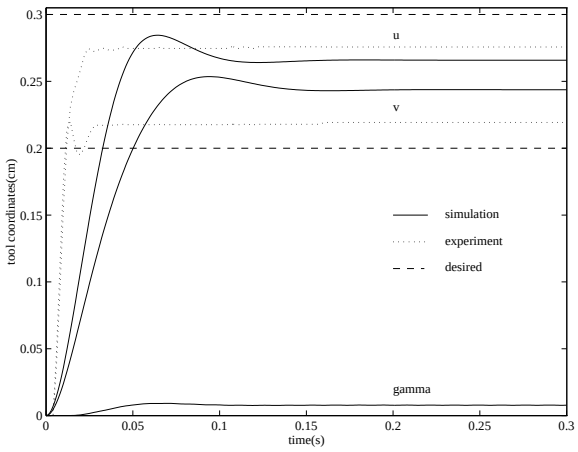

Figure 6: Position Step Response

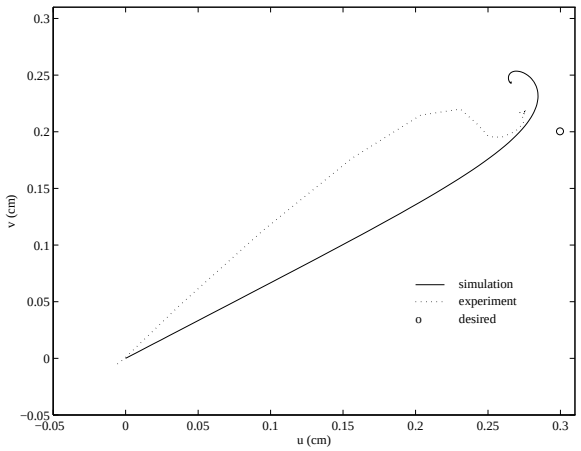

Figure 7: Position Step Response

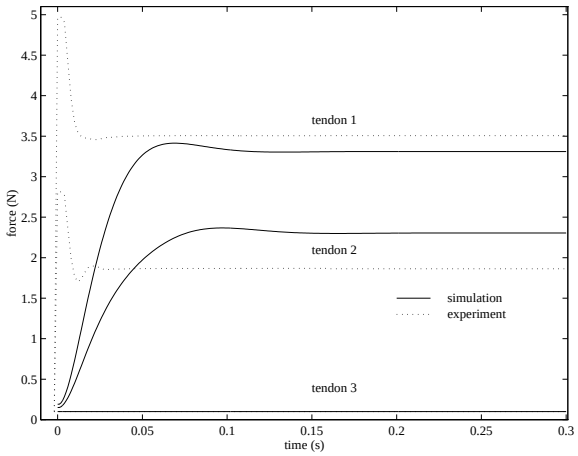

Figure 8: Tendon Force Step Response

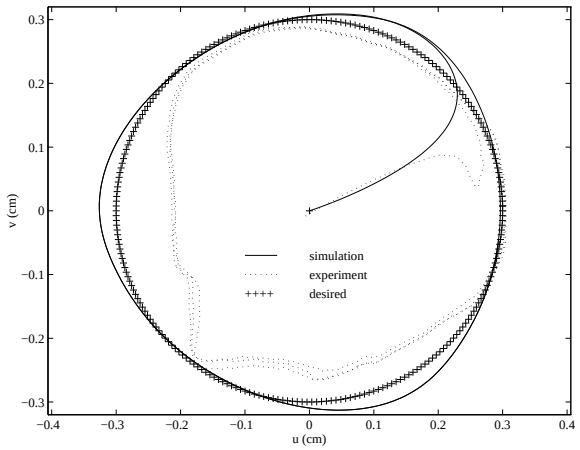

Figure 9: Circle Trajectory

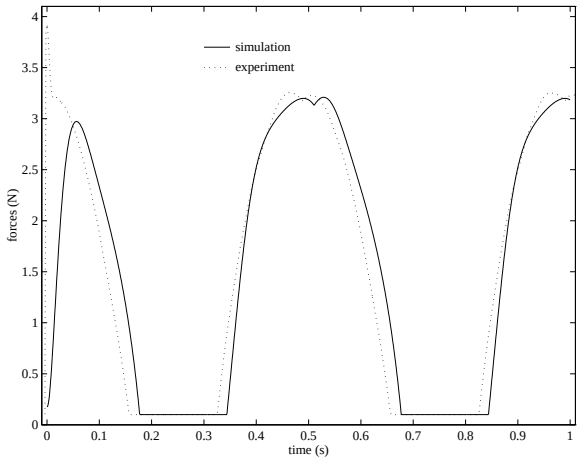

Figure 10: Force in Tendon A for 2.0 Hz Circle

The endo-platform is initially at the origin and the start point of the desired trajectory is $(u, v) = (0.3\text{cm}, 0.0\text{cm})$. The resulting trajectory in tool coordinates in the UV plane for the experimental system and the simulation is shown in Figure 9. The simulation does not completely follow the circle trajectory but deviates from the circle at three equally spaced angles. These angles correspond to the locations between the tendon attachments. This deviation is believed to be caused by the nonzero twist angle.

The experimental response for the circle significantly deviates from the desired trajectory in the lower left quadrant. This is believed to be caused by the spring constant being stronger in the $-u$ direction. Future design improvements are planned to eliminate the unsymmetric spring force. One could also modify the feedforward term to take into account the complicated spring force.

The forces for tendon A are shown in Figure 10 for the simulation as well as the experiment. The tendon force in the experiment is initially greater than the simulation which is attributed to the modified feedforward term in the experimental controller. After the initial deviation, the experimental and simulation forces differ slightly.

We are able to track circles at greater frequencies with the current controller. We have tracked circles at 20.0Hz where the radius of the experimental trajectory deviates between 0.11cm and 0.27cm. The deviation in the radius at 2.0Hz is between 0.21cm and 0.31cm. Currently, the forward kinematics algorithm fails after tracking a circle for more than 5 to 10 seconds. We are currently investigating this failure.

In the future, we plan on improving the mechanical design of our first prototype to improve the ability to track trajectories and to position endoscopic tools efficiently and reliably. We also plan on improving the control algorithm to improve its accuracy and reliability. Our first prototype has been instructive in the control and design of future endo-platforms.

6. Conclusion

This paper presents the kinematics, dynamics, and control of a recently designed endo-platform for endoscopy. Simulation as well as experimental results demonstrate the effectiveness of the controlled system to track step responses as well as circle trajectories. The workspace controller presented overcomes the difficulty imposed by the simple design since the device has the same number of degrees of freedom as tendons. The basic design has applications in addition to endoscopy. The design can be useful in targeting systems as well as snake-like robots. Future work involves improving the mechanical design and increasing the reliability and accuracy of the controlled system. We also plan on interfacing an improved prototype to an input device for use in medical experiments.

Thanks to Ed Nicolson, Brian Mirtich and Lara Crawford for their help in various aspects of this research.

7. References

[1] C. Deno, R. Murray, K. Pister, and S. Sastry. Finger-like biomechanical robots. ERL technical report, University of California at Berkeley, 1992. Department of EECS.

[2] J. Funda and R.P. Paul. A comparison of transforms and quaternions in robotics. In *IEEE International Conference on Robotics and Automation*, Philadelphia, 1988.

[3] S. Hirose. *Biologically Inspired Robots: Snake-Like Locomotors and Manipulators.* Oxford University Press, Oxford, 1993.

[4] MathWorks, Natick, Ma. *Matlab Reference Guide*, 1992.

[5] R. Murray, Z. Li, and S. Sastry. *A Mathematical Introduction to Robotic Manipulation.* CRC Press, Boca Raton, Fl, 1994.

[6] C. Nguyen, Z. Zhou, S. Antranzi, and C. Campbell. Efficient computation of forward kinematics and jacobian matrix of a stewart platform-based manipulator. In *IEEE Proceedings of SOUTHEASTCON*, Williamsburg, Va., 1991.

[7] J. Wendlandt. Milli robotics for endoscopy. ERL technical report, University of California at Berkeley, 1994. Department of EECS.

[8] S. Wolfram. *Mathematica: A System for Doing Mathematics by Computer.* Addison-Wesley, RedWood City, second edition, 1991.